Shape Evolution and Stress Development during Latex−Silica Film Formation

Carlos J. Martinez† and Jennifer A. Lewis*,†,‡

Materials Science and Engineering Department, Chemical Engineering Department, and The Beckman Institute for Advanced Science and Technology, Frederick Seitz Materials Research Laboratory, University of Illinois at Urbana-Champaign, Urbana, Illinois 61801

Received September 27, 2001. In Final Form: March 28, 2002

The shape evolution and stress development of composite films of deformable acrylic latices and rigid silica spheres were studied using noncontact laser profilometry and a controlled environment stress apparatus that simultaneously monitors optical clarity, drying stress, and weight loss. Their shape evolution was strongly influenced by capillary forces experienced during drying, latex T_g, and the ratio of deformable/rigid particles in the film. Their stress histories exhibited three distinct regions: (1) a period of stress rise stemming from capillary tension exerted by the liquid on the particle network, (2) a maximum stress, and (3) a period of stress decay. Significant differences in stress histories were observed between the deformable latex and rigid silica films. Latex films exhibited a gradual stress rise, a maximum stress of ∼0.1 MPa, and only a slight stress decay. In contrast, silica films displayed a sharp stress rise and a stress maximum of ∼1 MPa, followed by a decay to a nearly stress-free state at the culmination of the drying process. Composite films exhibited a marked transition from a deformable to a rigidlike response as their silica content increased above 40 vol %. The highest maximum stress was observed for composite films with 55% silica, which was near their critical pigment volume concentration. Such films also exhibited the highest amount of residual stress of all films studied.

Introduction

Latex and colloid-filled latex suspensions are used in numerous technological applications including ceramics processing, paints, coatings, paper, textiles, and adhesives. A hallmark of latex systems is their ability to coalesce at modest temperatures yielding a continuous film. Film formation, which occurs above the minimum film-forming temperature (MFT), has been studied for many decades.[1−10] The MFT is usually close to the glass transition temperature, T_g, of the polymer.[11] The film formation process can be divided into three stages. In stage I, latex-based suspensions undergo evaporation thereby increasing their solids content until a close-packed particle network forms. In stage II, this particle network undergoes deformation ideally leading to a densified structure without voids. Finally, in stage III, diffusion of polymer across the boundaries that arise between deformed latex particles yields a continuous film with mechanical integrity. Although the terms coalescence and film formation are often used interchangeably in the latex literature, Lin and Meier[12] offer the following definitions. They state that "coalescence" implies fusion of latex particles together by polymer interdiffusion, while "film formation" only implies that a film is formed by the distortion of particles to eliminate interstitial voids. Here, we utilize a more general definition of film formation that does not require, but may include, deformation leading to the complete elimination of voids. This definition is more suitable for films deposited from deformable and rigid colloids.

Latex-based systems can reside in the suspended, fully saturated, semidry, or dry state as film formation evolves. Initially, they reside in the suspended state, that is, there is excess water over that required to completely fill the pore space between close-packed latex particles, as shown in Figure 1. In this state, latex particles undergo Brownian motion analogous to suspensions of rigid colloidal particles and are free to migrate in response to capillary forces. As drying proceeds, the solids content increases until the particles form a touching network. The system is fully saturated when there is just enough water to completely fill the pore space between close-packed latex particles. This same definition holds for systems of rigid particles. Unlike latex particles, rigid colloids are unable to deform in response to capillary pressure arising from the water−air interfacial tension once this point is reached. Thus, upon further drying, films containing rigid particles begin to drain with larger pores opening first, followed by smaller ones. The semidry state occurs when porosity develops within such films. In contrast, latex particles can undergo deformation creating structural variations ranging from the saturated to semidry state as drying proceeds beyond their initial point of contact. For composite films comprised of both deformable and rigid colloids, the situation is more complicated. The liquid (and pore) distribution within the drying film depends on several parameters including the evaporation rate (v_e), the latex deformation rate, the length

* To whom correspondence should be addressed.
† Materials Science and Engineering Department.
‡ Chemical Engineering Department, and The Beckman Institute for Advanced Science and Technology, Frederick Seitz Materials Research Laboratory.

(1) Dillon, R. E.; Matheson, L. A.; Bradford, E. B. *J. Colloid Sci.* **1950**, *6*, 108−117.
(2) Brown, G. L. *J. Polym. Sci.* **1956**, *22*, 423.
(3) Bradford, E. B.; Vanderhoff, J. W. *J. Macromol. Chem.* **1966**, 335.
(4) Eckersley, S. T.; Rudin, A. *J. Coat. Technol.* **1990**, *61*, 89−100.
(5) Vanderhoff, J. W.; Tarkowski, H. L.; Jenkins, M. C.; Bradford, E. B. *J. Macromol. Chem.* **1966**, *1*, 361−397.
(6) Steward, P. A.; Hearn, J.; Wilkinson, M. C. *Adv. Colloid Interface Sci.* **2000**, *86*, 195−267.
(7) Visschers, M.; Laven, J.; German, A. L. *Prog. Org. Coat.* **1997**, *30*, 39−49.
(8) Winnik, M. A. *Curr. Opin. Colloid Interface Sci.* **1997**, *2*, 192−199.
(9) Cannon, L. A.; Pethrick, R. A. *Macrolecules* **1999**, *32*, 7617−7629.
(10) Keddie, J. L.; Meredith, P.; Jones, R. A. L.; Donald, A. M. *Macromolecules* **1995**, *28*, 2673−2682.
(11) Brodnyan, J. G.; Konen, T. J. *J. Appl. Polym. Sci.* **1964**, *8*, 687.
(12) Lin, F.; Meier, D. J. *Langmuir* **1996**, *12*, 2774−2780.

10.1021/la0114833 CCC: $22.00
Published on Web 05/15/2002

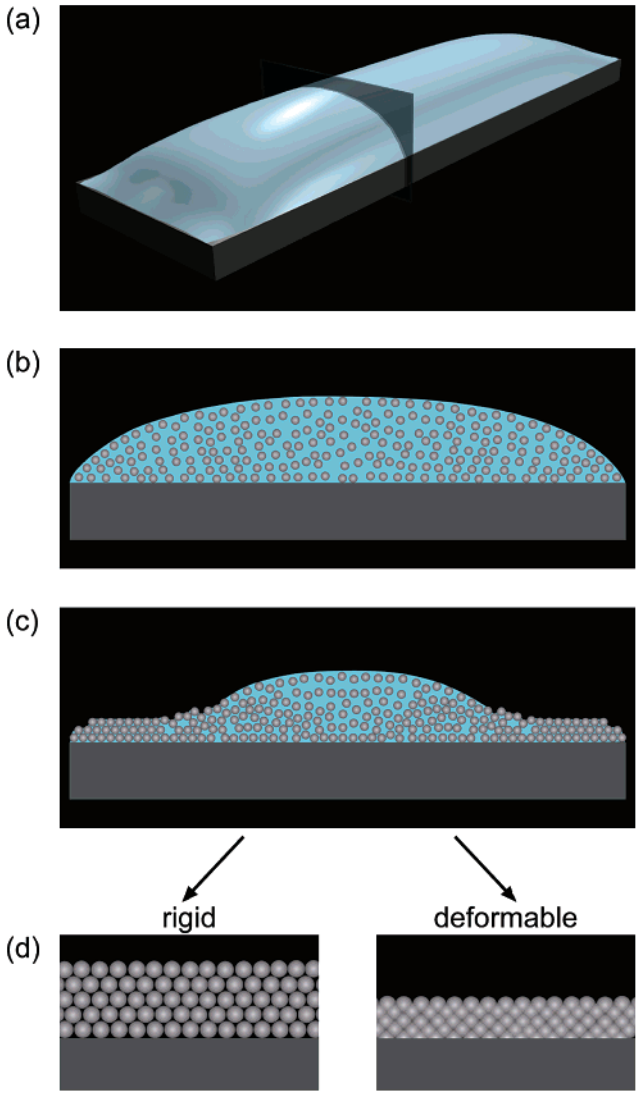

Figure 1. Schematic illustrations of shape evolution of rigid and deformable films during drying: (a) macroscopic view of deposited film on the substrate, (b) cross-sectional view of deposited film, (c) cross-sectional view of film after partial drying, and (d) cross-sectional view of films formed from rigid and deformable particles at the culmination of film formation.

scale over which capillary migration occurs, the film dimensions, and the ratio of deformable to rigid particles.

The shape evolution of latex-based films during drying is often considered to be spatially uniform. However, recent studies[13,14] have shown that lateral drying fronts can develop which move across the film from the edge inward. For latex films, the resulting lateral flow can affect the deformation process, as described by Winnik and Feng.[13] As the edge regions continue to dry, they wick water (and particles) laterally from the center of the film. An important consequence of lateral drying fronts in latex-based films is that particle deformation can be initiated at different times within a film of spatially varying thickness (or latex concentration). Routh and Russel[15,16] have developed a process model to predict the mechanism(s) by which film formation occurs for latex systems. They have cited the need for experimental observations that correlate shape evolution with the water content in such films during deformation.

Stress evolution during drying of latex-based films has received scant attention, despite its effects on film formation, defect generation (e.g., drying cracks), and delamination. Corcoran[17] carried out the first stress measurements on organic coatings using a cantilever deflection technique. Using this same approach, Perera[18,19] studied stress evolution in latex paints (with ∼50% pigment content) as a function of coating thickness. The internal stress was observed to increase with time until it reached a maximum value followed by modest decay. Although the time required to reach the maximum stress increased with coating thickness, the magnitude of the measured stress was independent of this parameter. Recently, Petersen[20] et al. extended the earlier work by Perera[18,19] studying both pure latex and colloid-filled latex films. They identified three distinct regions in the stress histories of such films, including an initial stress decline followed by a rise in stress and, ultimately, stress relaxation. Interestingly, they only attributed the initial stress decline, which they referred to as a dilational lateral stress, to the capillary pressure acting within the film. Their explanation seems unphysical, however, because the capillary pressure should only rise in a given film as the particle network forms (and the characteristic pore size decreases). Such effects were completely neglected by Petersen and co-workers, because they assumed that evaporation occurred quickly (∼1 min) relative to the time scale of their measurements.

Our aim is to investigate the shape evolution and stress histories of latex-based films produced from mixtures of deformable latex particles and rigid silica microspheres. We first present the behavior of films formed from individual constituents, which serves as a benchmark for interpreting the more complicated behavior of the composite films studied. For the first time, noncontact laser profilometry measurements were carried out on latex, silica, and the composite films to probe their 3-D shape evolution during film formation. These data were compared to predictions from shape evolution and process models developed by Parisse and Allain[21,22] and Routh and Russel,[15,16] respectively. Stress measurements were carried out in situ during the film formation process using a controlled environment cantilever deflection apparatus adopted from Payne and Francis.[23,24] We have modified their original design to permit concurrent measurements of film weight and optical clarity during this process. We present clear evidence that capillary forces and composition influence latex-based film formation. Our observations have important implications on the design of latex-based coatings for paints, paper, and tape casting of ceramic layers.

Experimental Section

Material System. Three acrylic latex emulsions (B-1035 and B-1001, Rohm & Haas Co., Philadelphia, PA, and DA-30NA, Dow Chemical Co., Midland, MI), with respective glass transition temperatures of −40, −6, and 19 °C, solids loadings of 55, 55,

(13) Winnik, M. A.; Feng, J. *J. Coat. Technol.* **1996**, *68*, 39−50.
(14) Routh, A. F.; Russel, W. B. *AIChE J.* **1998**, *44*, 2088−2098.
(15) Routh, A. F.; Russel, W. B. *Langmuir* **1999**, *15*, 7762−7773.
(16) Routh, A. F.; Russel, W. B. *Ind. Eng. Chem. Res.* **2001**, *40*, 4302−4308.
(17) Corcoran, E. M. *J. Paint Technol.* **1969**, *41*, 635−640.
(18) Perera, D. Y.; Eynde, V. *J. Coat. Technol.* **1984**, *56*, 47−53.
(19) Perera, D. Y. *J. Coat. Technol.* **1984**, *56*, 111−118.
(20) Petersen, C.; Heldmann, C.; Johannsmann, D. *Langmuir* **1999**, *15*, 7745−7751.
(21) Parisse, F.; Allain, C. *Langmuir* **1997**, *13*, 3598−3602.
(22) Parisse, F.; Allain, C. *J. Phys. II France* **1996**, *6*, 1111−1119.
(23) Payne, J. A. Stress Evolution in Solidifying Coatings. Ph.D. Thesis, University of Minnesota, Minneapolis, MN, 1998.
(24) Payne, J. A.; McCormick, A. V.; Francis, L. F. *Rev. Sci. Instrum.* **1997**, *68*, 4564−4568.

Table 1. Material Parameters

symbol	material	mean particle diameter [nm]	T_g [°C]	density [g/cm^3]
LT_g	B-1035	390	−40	1.05
MT_g	B-1001	330	−6	1.05
HT_g	DA-30NA	195	19	1.07
SiO_2	silica microspheres	570		2.25

and 61 vol %, and mean particle diameters of 390, 330, and 195 nm, served as deformable particles in this study. Their respective densities are 1.05, 1.05, and 1.07 g/cm^3. The surface tension of the solution phase in each latex suspension was measured by the Wilhelmy plate method.[25] All three solutions displayed a nearly identical value, and therefore an average surface tension of 39 dyn/cm is reported. Monodisperse silica microspheres (Geltech, FL) (570 ± 20 nm in diameter) with a density of 2.25 g/cm^3 served as model rigid particles. These material parameters are summarized in Table 1.

Suspension Preparation. Pure latex suspensions were prepared at a solids volume fraction (ϕ_{latex}) of 0.55. The suspension pH was adjusted to 9.0 ± 0.1 by adding an appropriate amount of hydrochloric acid (certified ACS plus, Fisher Scientific, Itasca, IL) or ammonium hydroxide (certified ACS plus, Fisher Scientific). Latex suspensions were magnetically stirred for 24 h at room temperature, after which their pH was readjusted if necessary.

Silica suspensions were prepared at a solids volume fraction (ϕ_{silica}) of 0.50 by adding an appropriate amount of silica microspheres to deionized water preadjusted to pH = 9.0. The suspensions were then ultrasonicated (Fisher Scientific 550 Sonic Dismembrator) at a 1 s on/off pulse interval for 300 s. The pH was adjusted to 9.0 ± 0.1 prior to magnetic stirring for 24 h and readjusted to 9.0 ± 0.1 after stirring, if necessary.

Binary suspensions of latex and silica microspheres were prepared with different latex/silica volumetric ratios at a total solids volume fraction (ϕ_{total}) of 0.50. Silica suspensions were first prepared by adding an appropriate amount of silica microspheres to deionized water preadjusted to pH = 9.0. The suspensions were then ultrasonicated (Fisher Scientific 550 Sonic Dismembrator) at a 1 s on/off pulse interval for 300 s. An appropriate amount of the as-received latex emulsion was then added, and the pH was adjusted to 9.0 ± 0.1, which yielded an optimal dispersion condition for both constituents. The suspensions were magnetically stirred for 24 h at room temperature, after which their pH was readjusted to 9.0 ± 0.1, as needed.

Shape Evolution of Films. Cross-sectional profiles of films analogous to those used in the stress measurements were obtained by a noncontact laser profilometer (model DRS2000, Cyber Optics, Minneapolis, MN). This profilometer employs a digital triangulation sensor that works by projecting a beam of light onto a film surface and calculating the distance from a reference point by determining where the reflected light falls on a pixelized-array detector. This noncontact method allows one to probe height changes during drying of wet films. The profilometer has a vertical resolution of ∼10 μm with a focal range of 2 mm. The laser profilometer was mounted on a z-axis stage, and the film of interest was attached to an $x-y$ computer-controlled stage. The distance between the profilometer and the sample was adjusted to reside in the middle of the profilometer focal range. A rectangular area (0.125 × 8.0 mm^2) was scanned using a step size of 0.025 mm every 45 s for a period of 90 min. All scans were carried out under ambient conditions (22−25 °C and 35−45% relative humidity (RH)).

Noncontact laser profilometry offers a facile method for characterizing the 3-D shape evolution of latex-based films during film formation. This technique is best suited for opaque films, because the measurement is based on detection of reflected light. Latex films undergo a transition from highly opaque to optically transparent, when film formation proceeds above the MFT.[26] Optical images of latex films formed from LT_g, MT_g, and HT_g latices were acquired by a digital video camera (Sony model DCR-TRV11, Japan) coupled to a computer. Digital images (not shown) were captured at 10 s intervals over a 5 h period to monitor their optical properties. During the first 90 min of film formation, each film maintained sufficient opacity required for profilometry measurements. Therefore, only these data are reported here. The LT_g films achieved optical clarity after 180 min, while the HT_g films required multiple days to achieve the same transparency. These measurements could have been extended throughout the film formation process by inclusion of a small amount of dye or opaque filler particles (e.g., silica microspheres) within the films.

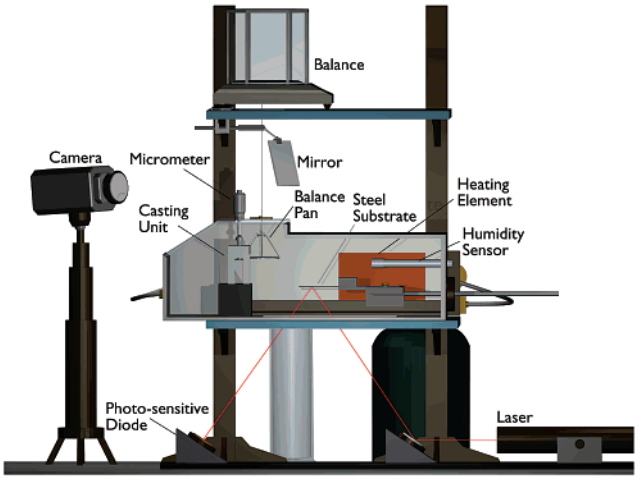

Figure 2. Schematic illustration of controlled environment experimental apparatus used for simultaneously measuring stress, weight loss behavior, and optical clarity of latex-based films. The external camera and mirror assembly enabled direct visualization of films (placed on balance pan) during the weight loss measurements.

Stress Histories of Films. The stress histories of films formed from pure latex, silica, and latex−silica suspensions were measured in situ during drying using the cantilever deflection technique illustrated in Figure 2. This device has an environmental chamber that allows for both humidity (15−70 RH ± 1%) and temperature (22−35 ± 1 °C) control. Additional specifications are provided elsewhere.[23,24] This technique relates the end deflection of a clamped stainless steel substrate to the stress developed in an attached coating as it dries. The end deflection was measured using an optical ensemble consisting of a 1 mW helium laser (Uniphase, model 1103), a position sensitive photodiode (UDT Sensors, no. DL-10), an array of mirrors, and a data acquisition computer. Clean, polished substrates were mounted onto a movable sample holder fixed at one end. A calibration curve for each substrate was obtained by deflecting the free end of the substrate a known distance using a micrometer. Using a propagation of error analysis, the measurement error for this apparatus in term of stress units was estimated to be ∼0.010 MPa. Upon calibration, the steel substrate was positioned beneath a small doctor blade and the suspension was deposited onto the substrate with a syringe. This assembly was then moved beneath the doctor blade at a constant speed of 1 cm/s to create a coating of the desired initial thickness (300 μm, unless otherwise specified). All films were dried at a 33% relative humidity and a temperature of 25 °C.

The biaxial, in-plane ($x-y$) stress, σ, averaged across the coating thickness is related to the substrate deflection by

$$\sigma = \frac{dEt_s^3}{3t_c l^2(t_s + t_c)(1-\nu)} + \frac{dE_c(t_s + t_c)}{l^2(1-\nu_c)} \quad (1)$$

where d, E, E_c, t_s, t_c, l, ν, and ν_c are the end deflection, elastic modulus of the substrate, elastic modulus of the coating, substrate thickness, film height, substrate length, Poisson ratio of the substrate, and Poisson ratio of the coating, respectively. If the modulus of the coating is much smaller than the substrate modulus (as is the case for most particulate films on rigid substrates), this second term can be neglected without introducing

(25) Pallas, N.; Pethica, B. *Colloids Surf.* **1983**, *6*, 221−227.
(26) Myers, R. R.; Schultz, R. K. *Polym. Sci.* **1964**, *8*, 755−764.

a significant error (~1% or less).[17,27] Therefore, only the first term in eq 1 was used for our stress data analysis. The stainless steel substrates used had a thickness of 209 μm and clamped dimensions of 50.8 mm × 6.35 mm with the following properties: $E = 190 \pm 20$ GPa, $l = 50.8$ mm, and $\nu = 0.36$.

There are several important considerations when applying the above equation to estimate internal stress development in latex-based films. First, the reported stress histories must be corrected to account for the contribution of weight loss associated with water evaporation to the measured deflection. Because the film height changes during the measurement, the instantaneous film height early in the experiment is greater than the final height. Despite the significant thickness variations observed initially, pure latex and silica films with mean final heights on the order of 100 μm are fairly uniform at the culmination of the film formation process. The reported stress histories have been calculated using a final film thickness, which represents an average value obtained by taking micrometer measurements across the entire sample. Use of this average value yields a reasonable estimate of the maximum and residual stress for a given film. In our experiments, the final film thickness exceeded ~$^1/_3$ of the substrate thickness. Payne[23] has shown that under these conditions the position of the neutral axis (plane in a bending plate where the strain is zero) within the coated substrate is shifted away from the location of $(t_s + t_c)/2$ assumed in eq 1 leading to a slight overestimate of the measured stress. Unfortunately, use of thinner films (or thicker substrates) reduced the signal-to-noise ratio considerably, making it difficult to obtain good data for the pure latex films. Finally, stress distributions throughout the coating thickness that arise due to microstructural differences cannot be measured by this technique. For example, local variations in the deformation rate across such films would impact their instantaneous modulus. However, this property is not included in the first term of eq 1. In related work, Smay and Lewis[28] have shown that there is little compositional variation (in the *z*-axis direction) in latex-based, composite films indicating the absence of microstructural differences in later stages of the film formation process. However, in light of the above considerations, the reported data should be viewed in a qualitative manner serving only as a guideline for establishing general trends between the films studied here.

Weight loss measurements were simultaneously carried out on duplicate samples in the cantilever stress chamber during the drying stress measurements. The weight loss data were acquired by suspending the coated substrate from a bottom-loading balance (Metler Toledo, model AG204). The sample mass was recorded every 10 s. Direct observations of latex coalescence were made by simultaneously imaging these samples during drying and film formation, as described above.

Results

Shape Evolution during Film Formation. The shape evolution of films deposited from pure latex suspensions of varying glass transition temperature is shown in Figure 3. To facilitate comparison, a series of representative 3-D slices obtained from a rectangular area (0.125 × 8.0 mm^2) acquired at several time intervals are shown alongside a complete sequence of 2-D slices for these films. The substrate scan, noted in each case, should be subtracted from a given film scan to yield the actual film shape. These films experienced dramatic shape changes as drying proceeded. The cross-sectional view illustrates their droplike shape (convex surface) analogous to the illustration depicted in Figure 1. The minimum film height was observed at the edges, with a maximum height found at or near the film center. As drying proceeded, both the center and edges of these films decreased in height. A hill-like feature, which extended along the film length, was observed at short times ($t \sim 15$ min) for all three films. The slope of this feature became more pronounced

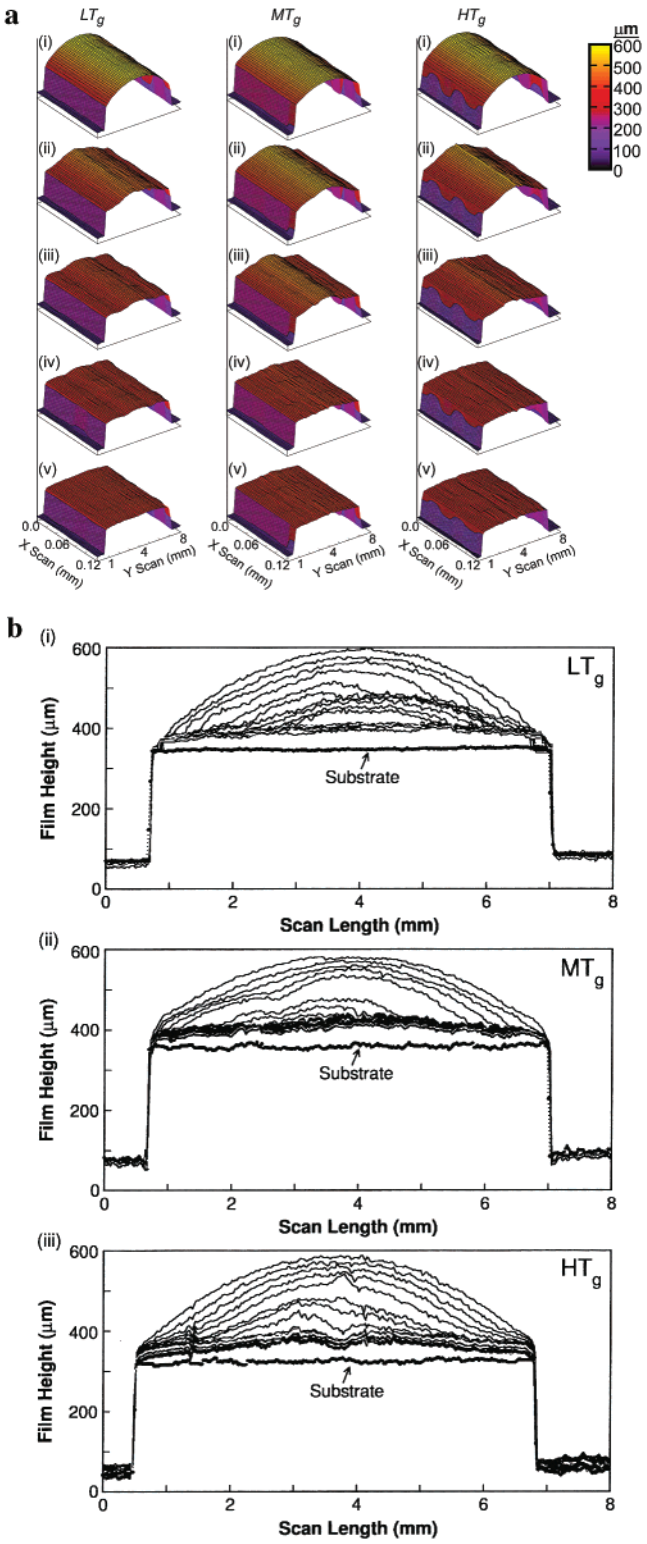

Figure 3. Shape evolution of latex films (cast height = 300 μm) of varying T_g; (a) 3-D images acquired at (i) 100%, (ii) 80%, (iii) 60%, (iv) 40%, and (v) 0% initial water content in the film and (b) 2-D image sequences of each film acquired at $x = 0.0625$ mm during film formation. [Note: The substrate scan corresponds to the bottom curve in each plot.]

as the latex T_g increased. At longer times ($t \sim 90$ min), the films achieved a nearly steady-state thickness that varied from the center to the edge regions. Films deposited from the HT_g latices contained a shallow valley that extended the entire film length at the culmination of this process. The depth of this valley was approximately 25 μm. Film

(27) Perera, D. Y.; Eynde, D. V. *J. Coat. Technol.* **1981**, *53*, 39−44.
(28) Smay, J. E.; Lewis, J. A. *J. Am. Ceram. Soc.* **2001**, *84*, 2495−2500.

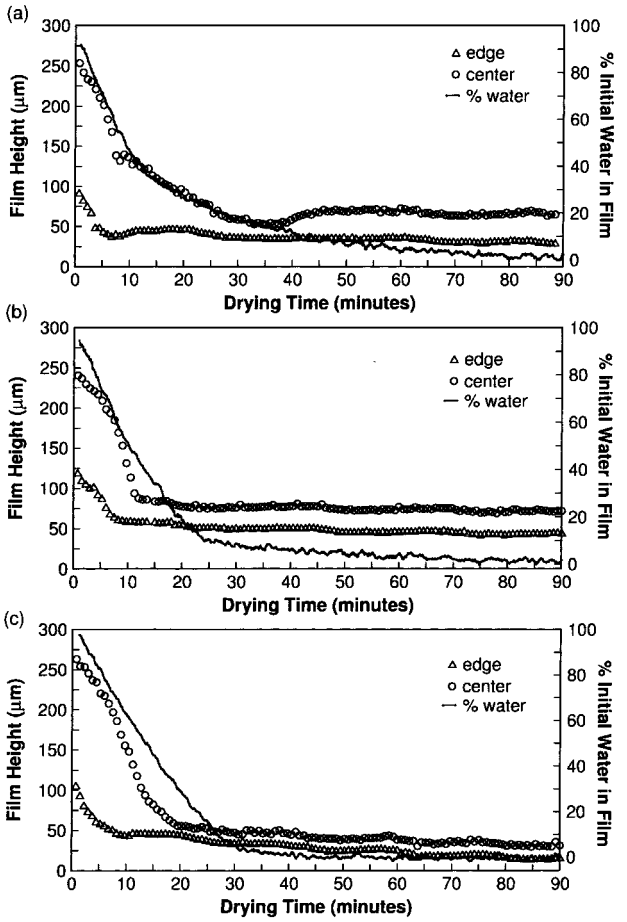

Figure 4. The film height and water content as a function of drying time for latex films (cast height = 300 μm): (a) LT_g, (b) MT_g, and (c) HT_g. [Note: Both center and edge heights of these films are shown.]

uniformity was enhanced as latex deformability increased, with the best results obtained for the LT_g films.

The film height in the center and edge regions is plotted as a function of time in Figure 4 for latex films of varying T_g. Each film exhibited initial center and edge heights of 250 ± 15 μm and 105 ± 15 μm, respectively, and final heights at 90 min of 65 ± 10 μm and 30 ± 15 μm, respectively. All films underwent the majority of their densification during the drying process. A constant rate period (CRP, $v_e = 4.5 \times 10^{-4} \pm 0.5$ g cm^{-2} min^{-1}) of evaporation was initially observed for these films. The CRP persisted until approximately 45%, 55%, and 70% of their initial water content was removed from the LT_g, MT_g, and HT_g films, respectively. During the CRP, the edge height attained a nearly steady-state value, with only a modest reduction observed beyond this point. In contrast, the center height did not approach a steady-state value until well beyond the CRP. Such differences are indicative of local variations in the deformation rate across the films. The rate of change of the center height was almost identical to the evaporation rate, especially for the lowest T_g film studied. A slow reduction in both the center and edge heights persisted after the drying process was complete for the highest T_g films studied.

The shape evolution of films deposited from MT_g latex−silica suspensions of varying composition is shown in Figure 5. The pure silica films shown in Figure 5 exhibited a droplike shape initially, with a minimum height observed at the film edges and a maximum height at the film center. A constant rate period ($v_e = 4.8 \times 10^{-4}$ g cm^{-2} min^{-1}) of evaporation was observed for these films throughout most of the drying process, that is, until ∼90% of their initial water content was removed. These films experienced only modest shape changes during the drying process due to their high initial solids content and the rigid nature of the particulate phase. The initial heights of the center and edge regions were 300 ± 15 μm and 130 ± 15 μm, respectively, whereas their heights at 90 min were 275 ± 15 μm and 100 ± 15 μm. As drying proceeded, a shallow valley developed in the film center that extended the entire film length.

Composite films deposited from mixtures of 40% silica or less exhibited behavior that was similar to that observed for pure latex films. As the ratio of rigid-to-deformable colloids increased, these composite films began to exhibit features analogous to those observed for rigid films. The most common similarity was the formation of a valley that extended the entire film length. Above 40% silica, film behavior was dominated by the rigid nature of the silica particles. The effects of the rigid particles are evident when examining the dependence of film height on composition, as shown in Figure 5b. The initial heights of center and edge regions were 265 ± 40 μm and 110 ± 15 μm, respectively. The center and edge heights at 90 min display only a modest compositional dependence for films with less than 40% silica. However, the center height increases nearly linearly with silica content beyond this concentration. The edge height also increases with silica content; however, this trend is less pronounced. Clearly, the extent of film densification decreases dramatically as the ratio of deformable latex to rigid silica particles approaches zero. The corresponding weight loss curves (not shown) indicated the presence of a constant rate period ($v_e = 4.5 \times 10^{-4} \pm 0.5$ g cm^{-2} min^{-1}) initially followed by a falling rate period. The total drying time decreased as the ratio of deformable (latex) to rigid (silica) particles in these composite films decreased, ranging from ∼70 to 20 min for silica contents between 20% and 80%.

Stress Evolution during Film Formation. The stress histories and corresponding weight loss behavior during formation of films deposited from latex suspensions of varying glass transition temperature are shown in Figure 6a. The latex films exhibited a period of rise in tensile stress (σ_{rise}) that extended throughout most of the weight loss period, that is, until ∼90% of the initial water was removed from the films. At this point, a maximum stress (σ_{max}) was reached, with values of 0.075, 0.098, and 0.105 MPa observed for LT_g, MT_g, and HT_g films, respectively. Little stress decay was seen beyond this point; therefore, their final stress (σ_{end}) at 90 min was nearly equivalent to the maximum stress experienced during film formation.

The stress histories of films prepared from silica suspensions are shown in Figure 6b. Significant differences in both the magnitude and form of the stress curves were observed between these films and the pure latex films. The silica films exhibited a rapid period of rise in tensile stress (σ_{rise}), followed by a maximum stress (σ_{max}) and a subsequent decay to a nearly stress-free state (σ_{end}). The period of stress rise culminated when the film reached a solids volume fraction of ∼0.58. A σ_{max} value of 0.91 MPa was found for these films. Beyond this peak stress, the stress decayed rapidly to yield a nearly stress-free state in the fully dry films.

The stress history of composite films prepared from binary (latex−silica) suspensions ($\phi_{total} = 0.50$) of varying composition is shown in Figure 7. Films assembled from latex−silica mixtures with 40% silica or less exhibited nearly identical stress histories. Their behavior was

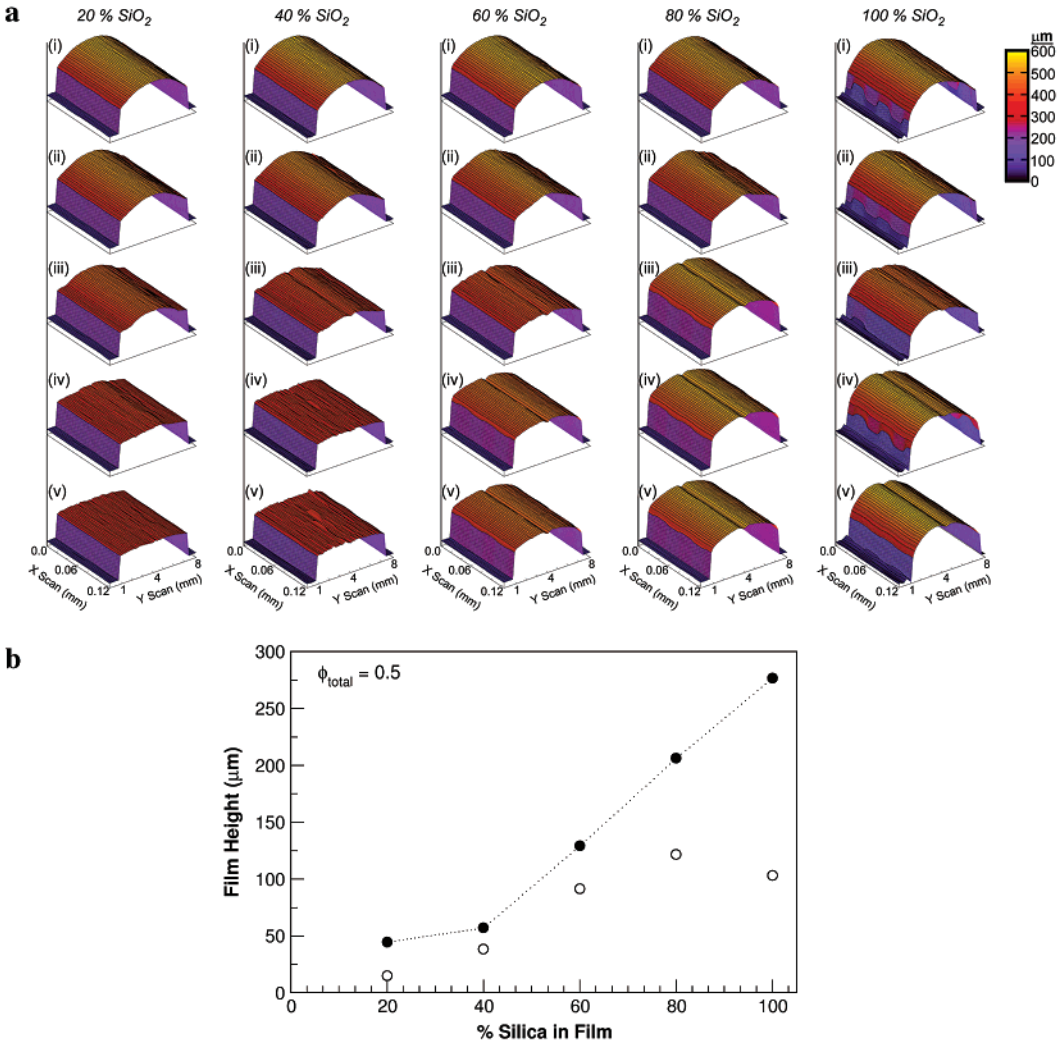

Figure 5. Shape evolution of MT_g−silica films (cast height = 300 μm) of varying composition: (a) 3-D images acquired at (i) 100%, (ii) 80%, (iii) 60%, (iv) 40%, and (v) 0% initial water in the film and (b) film height (t = 90 min) in the center (●) and edge (○) regions as a function of silica content. [Note: To facilitate comparison of these data, a constant initial film height was used even though this exceeded the critical cracking thickness of the pure silica films (ref 34).]

indistinguishable from that observed for pure latex films. As the relative percent of silica was further increased, however, a dramatic change in their stress evolution was observed. At 45% silica, there was a slight appearance of a sharper peak in the maximum stress at a drying time of 20 min. This peak became even more pronounced for films assembled from latex−silica mixtures with 50% silica or higher. Both the period of stress rise and the stress decay following the maximum stress decreased becoming increasingly sharper with higher silica content.

Discussion

Our experimental observations reveal that the shape evolution and stress development in latex-based films are strongly influenced by capillary forces, latex T_g, and the ratio of deformable/rigid particles in the film. We begin by discussing their shape evolution, with emphasis given to the deformation mechanisms experienced by pure latex films of varying T_g during film formation. Next, we address the effects of rigid particles on their shape evolution. Finally, we discuss the origin of stress development in pure and composite films during the film formation process.

Shape Evolution of Latex-Based Films. Shape evolution of latex-based films is governed by both water evaporation and particle deformation processes. In the absence of particle deformation, water evaporation produced only a modest shape change (see Figure 5) for the pure silica films studied here. We attribute this behavior to their high initial solids loading ($\phi \geq 0.5$). In contrast, pure latex films experienced significant shape changes despite similarities in their initial solids content, which indicates that latex deformation has occurred during film formation.

Several mechanisms have been proposed in the literature to describe latex deformation, including wet sintering,[5,29] dry sintering,[1,30] capillary deformation,[2,4] receding water front,[4,10] and Sheetz deformation.[31] The first two mechanisms represent limiting cases. In wet sintering, latex deformation is independent of water evaporation. The process is driven solely by the polymer−water interfacial energy. In dry sintering, latex deformation is not initiated until water evaporation is completed and is driven by polymer−vapor interfacial energy. The other mechanisms lie between these two limits. Capillary deformation involves simultaneous removal of water from

(29) Dobler, F.; Pith, T.; Lambla, M.; Holl, Y. *J. Colloid Interface Sci.* **1992**, *152*, 1−11.
(30) Sperry, P. R.; Snyder, B. S.; O'Dowd, M. L.; Lesko, P. M. *Langmuir* **1994**, *10*, 2619−2628.
(31) Sheetz, D. P. *J. Appl. Polym. Sci.* **1965**, *9*, 3759−3773.

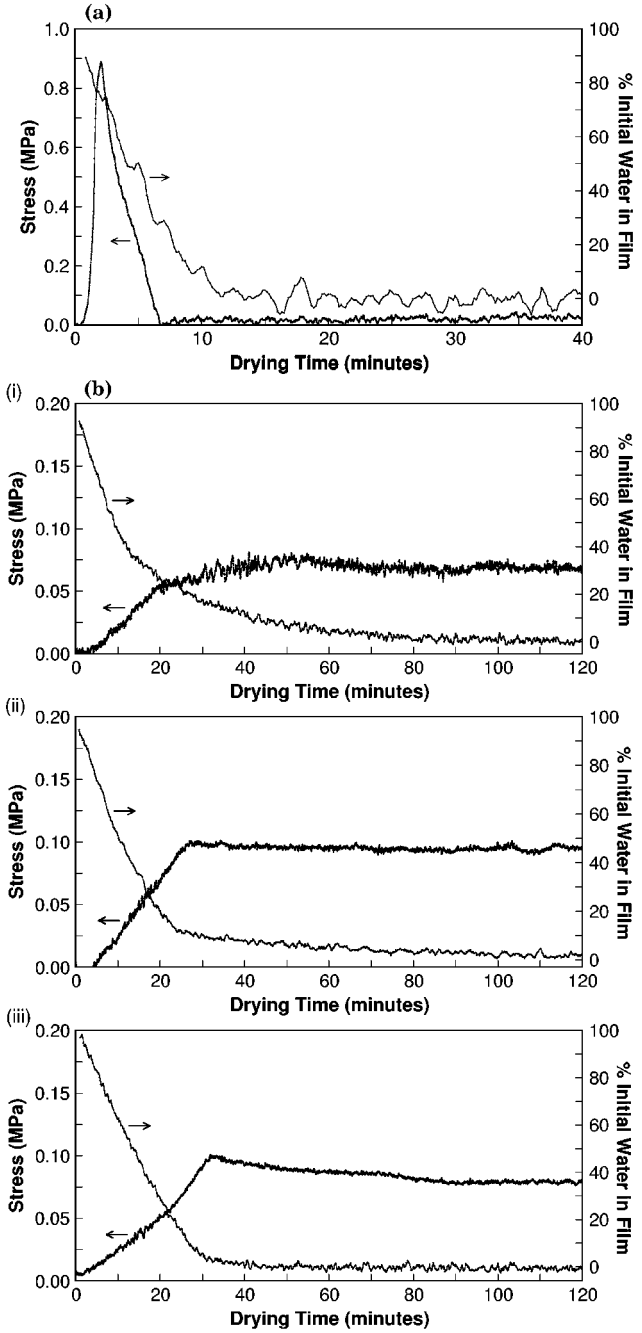

Figure 6. The stress histories and water content as a function of drying time for (a) silica films (cast height = 100 μm) and (b) latex films (cast height = 300 μm): (i) LT_g, (ii) MT_g, and (iii) HT_g.

the film and latex deformation. This process is driven by the capillary tension that develops in the liquid phase due to curvature at the water−vapor interface. Keddie et al.[10] was first to identify the receding water front mechanism, which occurs when latex deformation is not complete by the time the capillary pressure reaches a maximum value. After the liquid menisci retreat into the film, further latex deformation occurs by the dry (or moist) sintering mechanism. Finally, Sheetz deformation arises when a vertical inhomogeneity in latex concentration develops within the film, as water evaporation proceeds. The buildup of latex particles at the air−film interface may lead to skinning effects, which hinder evaporation.

Routh and Russel[15,16] have recently developed a process model to predict the controlling mechanism(s) during latex

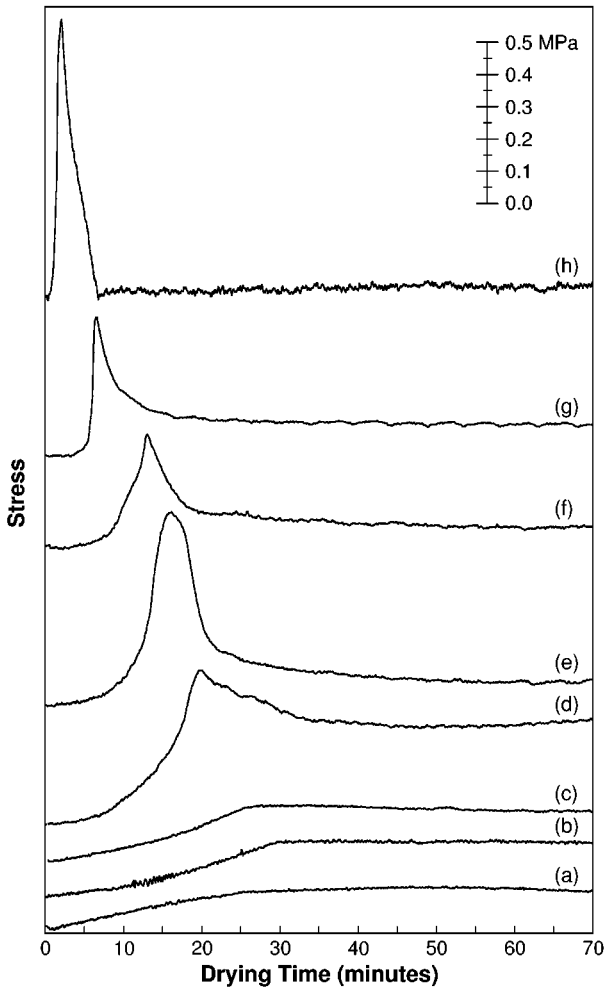

Figure 7. The stress histories of MT_g−silica films of varying composition: (a) 0%, (b) 20%, (c) 40%, (d) 50%, (e) 55%, (f) 65%, (g) 75%, and (h) 100% silica. [Note: Films were cast at varying initial heights to produce average final heights of ~100 μm.]

film formation. They defined several dimensionless parameters, the most important of which is given by

$$\bar{\lambda} = \frac{\eta_0 a_0 v_e}{\gamma H} \tag{2}$$

where η_0 is the low shear viscosity, a_0 is the initial particle radius, γ is the surface tension of the liquid−vapor interface, and H is the initial film height. $\bar{\lambda}$ relates the time required for viscous deformation to an evaporation time, $t = v_e/H$. They predict that film formation occurs by wet sintering for $\bar{\lambda} < 1$, capillary deformation for $1 < \bar{\lambda} < 10^2$, a receding water front for $10^2 < \bar{\lambda} < 10^4$, and dry (or moist) sintering for $\bar{\lambda} > 10^4$. To evaluate the possibility of inhomogeneous drying (Sheetz mechanism), one must determine the Peclet number (Pe), which relates the evaporation rate to diffusion. The Pe is given by Hv_e/D_0, where $D_0 = kT/6\pi\eta a_0$ and η = solution viscosity.[15,16] When the Peclet number is large ($\gg$1), skinning can occur during film formation.

We calculated the $\bar{\lambda}$ and Pe values reported in Table 2 for our latex films using the equations described above. The LT_g and MT_g films were both predicted to undergo deformation by wet sintering, whereas the HT_g films were predicted to undergo deformation by the receding water front/capillary deformation mechanisms. Given that Pe > 1, it is possible that inhomogeneous drying (Sheetz mechanism) could occur in any of these films. Discerning

Table 2. Predicted Mechanisms of Latex Deformation

sample	T [°C]	R_0 [nm]	$T - T_g$ [°C]	η_0 [Ns/m^2]	Pe	$\bar{\lambda}$	mechanisms predicted
LT_g	−40	195	65	3.9×10^3	15.3	3.7×10^{-6}	wet sintering
MT_g	−6	165	31	6.8×10^6	12.9	5.5×10^{-3}	wet sintering
HT_g	19	97.5	6	2.3×10^{11}	7.7	109	capillary deformation/receding water front

the relative importance of these various mechanisms solely from shape evolution data is difficult. For example, the external film shape would be similar whether wet sintering or capillary deformation occurred provided the films dry homogeneously. By coupling experimental observations of their shape evolution and water content (see Figure 4) with their optical property evolution (images not shown), we find reasonable agreement with the predicted behavior. For example, our observations suggest that the LT_g films experience capillary deformation, wet sintering, and Sheetz deformation during film formation. The excellent correlation between the film height (center region) and water content decreases in the film implies that capillary deformation has occurred. The premature transition from a constant rate period to a falling rate period (FRP) of water evaporation, observed when ∼45% of the initial water was removed from the film, implies that the particle deformation rate exceeded the evaporation rate (wet sintering) leading to enhanced particle deformation at the film surface (a hallmark of the Sheetz mechanism). Our experimental observations for the MT_g films also suggest that capillary deformation, wet sintering, and, to a far lesser extent, Sheetz deformation occurred during film formation. For the MT_g films, the onset of enhanced particle deformation at the film surface, as reflected by the CRP to FRP transition, was not observed until ∼55% of the initial water was removed from the film. For these films, the suppression in the evaporation rate seen beyond this transition was far less than that of the LT_g films. Both LT_g and MT_g films experienced negligible changes in shape and were optically transparent after water removal was complete. These observations suggest that dry sintering was not relevant. In contrast, our observations of the HT_g films indicate that capillary deformation initially dominates their formation followed by a modest amount of dry (or moist) sintering. There was little evidence of polymer skinning, as a CRP was maintained throughout most of the drying process. The majority of film densification occurred for the HT_g films during drying; however, some densification was observed beyond this point. This observation combined with the fact that these films required several hours to achieve optical clarity is strong evidence that dry sintering plays an important role in these films.

The morphological changes that occur during drying of planar films and drops formed from pure latex and pure silica suspensions have been studied previously.[21,22,32−35] For example, Ciampi et al.[33] have studied the shape evolution of latex films by mapping their water distribution both laterally and vertically using magnetic resonance imaging. This technique allows one to follow the local distribution of water in the films, although the external film shape cannot be imaged once significant water evaporation has occurred. Their work has helped elucidate the effects of lateral drying in latex films. Water evaporation alone has been shown to induce significant shape changes in colloidal films when their initial solids content is low.[21,22,32−34] For example, Parisse and Allain[21,22] have studied the shape evolution during drying of drops prepared from pure silica suspensions ($\phi_{silica} = 0.24$). These drops exhibited a spherical cap shape initially. As drying proceeded, the drop base remained constant, whereas distortions from the spherical cap shape were observed as a solid foot (or ring) formed at the drop periphery. They derived expressions relating the lateral flux of water in the drying drop based on simple shape models that maintained a constant angle at the drop−substrate interface or a constant base area. We did not observe the pronounced formation of a foot (or ring) region in pure silica films studied here, because they were produced from highly concentrated suspensions ($\phi \geq 0.5$). Due to sample geometry differences, their shape evolution is not compared to models developed by Parisse and Allain.[21,22] However, the formation of a valley that extended the entire film length (see Figure 5) is strong evidence of lateral drying effects.[34] For the composite films studied, we observed a transition from deformable to rigidlike behavior with increasing silica volume fraction. The onset of this transition coincided with a change in continuity between these two phases, as discussed in the next section.

Stress Evolution of Latex-Based Films. Stress develops during film formation because of the constrained volume shrinkage associated with loss of water from these films and particle deformation. Because no external loads are applied during this process, mechanical equilibrium requires that the capillary tension developed in the liquid phase exert a compressive force of equal magnitude on the particle network.[4,34] Since the drying film adheres strongly to the underlying substrate, its contraction occurs only in the z-direction, perpendicular to the film plane (see Figure 1). The capillary pressure (P_{cap}) in the liquid is given by Laplace's equation:[36]

$$P_{cap} = \frac{2\gamma}{r_p} \tag{3}$$

where γ is the liquid/vapor surface tension and r_p is the characteristic pore size. During film formation, evaporative processes lead to an increased solids volume fraction and corresponding decrease in characteristic pore size within the film. This pore radius, r_p, can be approximated by the hydraulic radius, r_h[36]:

$$r_h = \frac{2(1-\phi)}{\phi \rho_s S} \tag{4}$$

where ϕ is the colloid volume fraction, ρ_s is the theoretical density of the colloidal phase, and S ($= 6/D\rho$, D = mean particle diameter) is the specific surface area. Using these equations, one estimates a $P_{cap} \sim 1$ MPa for the latex-based films studied here. As water evaporation occurs, the films undergo a transition from the suspended to the saturated state bringing the particles into close contact with one another. A particle network comprised of rigid spheres can ultimately support this capillary pressure when its maximum solids loading is reached. This

(32) Deegan, R. D.; Bakajin, O.; Dupont, T. F.; Huber, G.; Nagel, S. R.; Witten, T. A. *Nature* **1997**, *389*, 827−829.
(33) Ciampi, E.; Goerke, U.; Keddie, J. L.; McDonald, P. J. *Langmuir* **2000**, *16*, 1057−1065.
(34) Guo, J. J.; Lewis, J. A. *J. Am. Ceram. Soc.* **1997**, *82*, 2345−2358.
(35) Salamanca, J. M.; Ciampi, E.; Faux, D. A.; Glover, P. M.; McDonald, P. J.; Routh, A. F.; Peters, A. C. I. A.; Satguru, R.; Keddie, J. L. *Langmuir* **2001**, *17*, 3202−3207.
(36) Smith, D. M.; Scherer, G. W.; Anderson, J. M. *J. Non-Cryst. Solids* **1995**, *188*, 191−206.

coincided with a $\phi_{silica} \sim 0.58$ for the pure silica films.[34] In contrast, a particle network comprised of deformable latex particles will continue to densify in response to the tension in the liquid phase provided the film is held above its MFT. Ideally, such films can achieve a ϕ_{latex} of unity, as shown in Figure 1d.

The observed stress histories of the pure and composite films were influenced by both the capillary forces and shape evolution experienced during film formation. We begin by discussing the behavior observed for the pure silica films, which serves as a benchmark for understanding the more complicated behavior of the latex-based films. The silica films exhibited an initial period of stress rise that reflects the buildup of capillary pressure as particle network formation occurs. This period of stress rise was rapid, because very little water evaporation occurred before $\phi_{silica} \sim 0.58$, where the maximum stress was observed. A maximum stress σ_{max} of 0.91 MPa was found, which was in excellent agreement with the estimated capillary pressure P_{cap} of 0.97 MPa for these films. The period of stress decay following the observed maximum drying stress occurred when liquid menisci retreated into the films, that is, as their degree of saturation fell below 100%. Upon the culmination of the drying process, the stress decayed to a negligible value. Their total drying time was much less than that observed for the pure latex films due in part to their lower initial film height and to the fact that a continuous pore network existed in these films throughout drying.[34]

The stress histories of the pure latex films differed significantly from those observed for the rigid silica films. The latex films exhibited a period of gradual stress rise to a maximum value of ~0.1 MPa despite similarities in their initial solids loading and particle size. We estimated P_{cap} to be ~1.2 MPa using an average surface tension of 39 dyn/cm, $\phi_{latex} = 0.64$, and mean particle size of 330 nm. This predicted maximum stress was never achieved during film formation, because the particle network could undergo deformation in response to the tension in the liquid phase. The measured stress was therefore influenced not only by capillary forces but also by stress relaxation process(es)[15,37] that occur during film formation. Modest differences in maximum stress observed between the latex films indicate, as expected, that their ability to relax stress was hindered with increasing T_g.[38]

The stress histories of the composite films exhibited features characteristic of both the rigid silica and deformable latex films. The behavior of composite films assembled from latex−silica mixtures with 40% silica or less was nearly indistinguishable from that of the pure latex films. With increasing silica content, their behavior began to display features associated with rigid films. The dependence of the maximum and final stress values on silica volume fraction is shown in Figure 8 for these composite films. The highest maximum stress was observed for films with $\phi_{silica} \sim 55$, which correlates well to the maximum packing fraction observed at the culmination of the drying process. Near this value, there was also a 3-fold increase in the final stress, suggesting that stress relaxation processes were significantly altered for composite films in this compositional range.

The physical properties of latex-based coatings that contain rigid particles, such as inorganic fillers and pigments or blends of low and high T_g latices,[13,39] are known

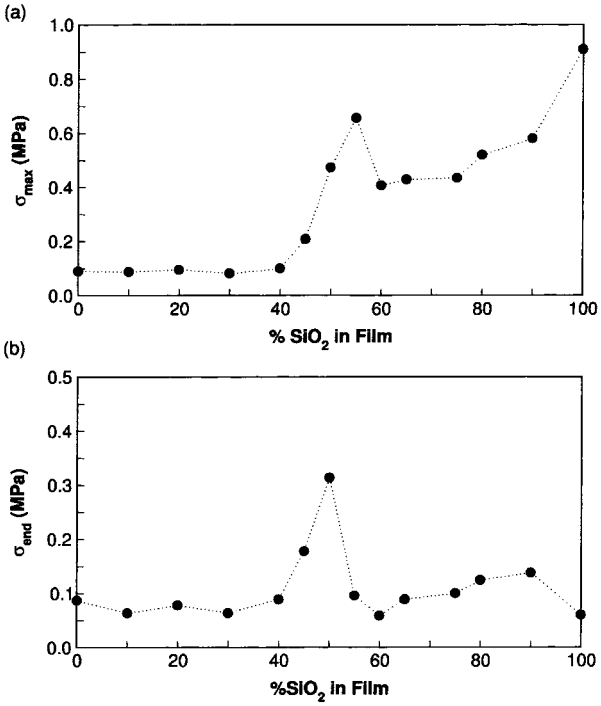

Figure 8. The (a) maximum film stress (σ_{max}) and (b) final film stress (σ_{end}) as a function of silica content for MT_g−silica films of varying composition.

to depend strongly on the continuity of the individual phases.[40] One can estimate the critical volume fraction (ϕ_c) at which the silica phase becomes continuous in the MT_g latex−silica films by one of two approaches. By treating these films as binary mixtures of spherical particles of varying size, one can invoke models developed by Kusy[41] and applied to films formed from latex blends by Eckersley and Helmer[42] to estimate ϕ_c. We calculated ϕ_c of 0.53 (ideal case) and 0.7 (nonideal case) for binary mixtures of MT_g latex particles and silica microspheres of radius ratio, a_{latex}/a_{silica}, equal to 0.58. The difficulty with this approach is that the Kusy models do not explicitly account for latex deformation and therefore yield values that are qualitative at best. Alternately, one can invoke the concept of a critical pigment volume concentration (CPCV) defined as the point where there is sufficient polymer to just wet and fill the interstices between rigid particles.[39,43] Based on our observations, the CPCV occurs at $\phi_{silica} \sim 0.58$ for these films. Composite films with ϕ_{silica} greater than ~0.58 contained internal porosity, whereas those with ϕ_{silica} less than ~0.58 consisted of silica particles embedded within a continuous polymer matrix. Clearly, we observed dramatic changes in the shape evolution and stress histories of these composite films near the CPCV.

Summary

The shape evolution and stress development of latex-based films during film formation has important consequences on final film quality and properties. We studied such processes by simultaneously monitoring the shape evolution, optical clarity, weight loss, and drying stress of films of varying composition and found that both capillary phenomena and compositional effects play

(37) Bellehumeur, C. T.; Kontopoulou, M.; Vlachopoulos, J. *Rheol. Acta* **1998**, *37*, 270−278.
(38) Pekcan, O.; Capolat, M. *J. Appl. Polym. Sci.* **1997**, *63*, 651−659.
(39) Feng, J.; Winnik, M. A.; Shivers, R. R.; Clubb, B. *Macromolecules* **1995**, *28*, 7671−7682.
(40) Tzitzinou, A.; Keddie, J. L.; Geurts, J. M.; Peters, A. C. I. A.; Satguru, R. *Macromolecules* **2000**, *33*, 2695−2708.
(41) Kusy, R. P. *J. Appl. Phys.* **1997**, *48*, 5301−5305.
(42) Eckersley, S. T.; Helmer, B. J. *J. Coat. Technol.* **1997**, *69*, 97−107.
(43) Bierwagen, G. P. *J. Paint Technol.* **1972**, *44*, 46−55.

important roles. We found that their shape evolution was strongly influenced by the capillary forces experienced during drying, latex T_g, and ratio of deformable/rigid particles. Their stress histories were complex exhibiting a strong compositional dependence. In sharp contrast to the recent work by Petersen et al.,[20] we only observed an initial tensile stress rise in such films in response to the capillary forces generated during the drying process. Composite films containing greater than 40% silica exhibited an increasingly rigidlike response with increased filler content. Films assembled near the critical filler (silica) volume concentration exhibited the highest stresses of all composite films studied. Our observations have important implications for the design of latex-based coatings based on blends of deformable and rigid particles, albeit organic/inorganic mixtures or organic blends of varying T_g, as well as for future measurements and modeling of stress development in such films.

Acknowledgment. The authors thank L. Francis for valuable discussions, J. Payne and L. Francis (U. Minnesota) and J. Smay (UIUC) for their assistance with the design and building of our drying stress apparatus, and E. Mikalsen for his experimental assistance. Funding for this research was provided by NASA (NAG# 8 − 1471). C. J. Martinez was partially funded by an IMGIP and SURGE Fellowships.

LA0114833